*Int. J. Electrochem. Sci.*, 17 **(2022)** Article Number: 221226, doi: 10.20964/2022.12.24

International Journal of
ELECTROCHEMICAL
SCIENCE
www.electrochemsci.org

# Cerium chloride and L-arginine as effective hybrid corrosion inhibitor for 5052 aluminum alloy in 3.5% NaCl solution

*X.T. Xu*[1,2], *H.W. Xu*[1,2], *Y. Wang*[1,2], *X.Y. Zhang*[1,2*], *X.J. Tan*[1,2,*]

[1] School of Mechanical Science and Engineering, Northeast Petroleum University, 199 Fazhan Road, Daqing 163318, P.R. China
[2] Heilongjiang Key Laboratory of Petroleum and Petrochemical Multiphase Treatment and Pollution Prevention, Daqing 163318, Heilongjiang, China
[*]E-mail: zxydqpi@sina.com, 1259946915@qq.com

*Received:* 8 October 2022 / *Accepted:* 27 October 2022 / *Published:* 17 November 2022

In this paper, experimental and theoretical methods were combined to study the corrosion inhibition behavior of a hybrid cerium chloride ($CeCl_3$) and L-arginine (L-Arg) inhibitor for 5052 aluminum alloy in 3.5% NaCl solution. Weight loss test results showed the highest inhibition efficiency was 83.78% when 3 mM $CeCl_3$ and 4 mM L-Arg were added. Polarization curve results showed the hybrid inhibitor was a mixed-type inhibitor. In the optimal concentration, the $E_{pit}$ increased by 208 mV compared with that of blank solution, which significantly improved the pitting corrosion resistance of 5052 aluminum alloy. Additionally, the electrochemical impedance spectroscopy results indicated the hybrid corrosion inhibitor effectively increased the charge transfer resistance, which hindered the corrosion process. Crystal morphology calculation showed the most stable surface of $CeO_2$ was {111} surface and the Monte Carlo simulation results showed $CeO_2$ film increased adsorption energy of L-Arg molecules compared with $Al_2O_3$ film. Combining the experimental and theoretical results, the inhibition ability of the hybrid inhibitor was attributed to the formation of $CeO_2/Al_2O_3$–L-Arg complex films, which dramatically hindered the diffusion of $Cl^-$ and blocked active sites of corrosion reaction.

**Keywords:** Aluminum alloy; Corrosion inhibitor; NaCl solution; Monte Carlo simulation; Pitting corrosion

## 1. INTRODUCTION

5052 aluminum alloy is widely used in construction [1], shipping [2], battery [3] and automobile [4] fields given the low density, outstanding specific strength, and low price [5, 6]. Generally, a dense and stable $Al_2O_3$ film is formed on aluminum alloy surface, which makes it exhibits well corrosion resistance [7, 8]. However, in an environment containing corrosive $Cl^-$ (such as marine environment),

the $Al_2O_3$ film will be damaged and lead to severe pitting corrosion [9], which limits the application of 5052 aluminum alloy.

The addition of corrosion inhibitors to a corrosive environment is a low-cost, high-efficiency, and easy-operation method to improve corrosion resistance for aluminum alloy [10, 11]. However, traditional heavy metal salt inhibitors, such as chromates, are toxic and harmful to the environment [12, 13]. Therefore, the development of non-toxic and environment friendly corrosion inhibitors has attracted increasing attention [14-16]. Studies [17, 18] showed that rare earth salts are promising and environment friendly corrosion inhibitors for various environments. Among them, cerium salts are highly efficient as corrosion inhibitors [19, 20]. Deyab et al. [21] investigated the corrosion inhibition effect of cerium chloride and cerium sulphate, and found that both inhibitors increased the pitting corrosion resistance of AA6061 aluminum alloy. Other studies revealed that a hybrid corrosion inhibitor consisting of rare earth salts and organic inhibitors can reach higher inhibition efficiency than a single corrosion inhibitor. [22]. Among organic corrosion inhibitors, amino acids are environment friendly [23], and have rich material source [24]. Previous study found that L-arginine (L-Arg) is an amino acid with potential to be an environment-friendly [25] and effective inhibitor in an environment containing $Cl^-$ [26]. However, research on the combination of cerium salt and L-Arg as a hybrid corrosion inhibitor for 5052 aluminum alloy is lacking.

Theoretical studies at the atomic level are also needed to systematically reveal the inhibition mechanism of hybrid inhibitor [27]. Monte Carlo (MC) calculation is useful to reveal the most stable adsorption configuration and relative adsorption energy for corrosion inhibitor particles [28]. Many studies [29, 30] have proven it is a powerful tool to reveal corrosion mechanism at the atomic level. Therefore, the combination of experimental and theoretical research is useful to systematically reveal the corrosion inhibition mechanism and develop various inhibitors.

In this paper, experimental and theoretical methods were combined to study the corrosion inhibition behavior of a novel $CeCl_3$ and L-Arg hybrid corrosion inhibitor for 5052 aluminum alloy in 3.5% NaCl solution. Experimental research included weight loss test, electrochemical test, surface morphology, and element composition test. Theoretical research included crystal growth morphology and MC calculation. Finally, the inhibition mechanisms were revealed. This research can offer some reference to develop similar hybrid corrosion inhibitors in environment which containing $Cl^-$.

## 2. MATERIALS AND METHODS

### *2.1. Materials*

In this study, all specimens were cut by spark wire cutting machine from 5052 aluminum alloy. The NaCl and $CeCl_3$ were analytical reagents, the L-Arg were biological reagents. Deionized water was used to prepare electrolyte solution.

*2.2. Weight loss test*

The samples with dimension of 4 × 4 × 0.3 cm were grounded by SiC abrasive paper from 400 to 2000 grit, then ultrasonic washed in anhydrous ethanol. The cleaned samples were immersed in 3.5 % NaCl solution without or with different corrosion inhibitors for 7-day. After 7-day test, samples were washed by distilled water and anhydrous ethanol. The mass of samples before and after testing were measured by analytical balance ($10^{-4}$ g accuracy). The corrosion rate ($v$) was determined by Eq. (1):

$$\boldsymbol{v} = \frac{\boldsymbol{m_1 - m_2}}{\boldsymbol{s \times t}} \quad (1)$$

the $\boldsymbol{m_1}$ is the mass (mg) of sample before testing, $\boldsymbol{m_2}$ is the mass (mg) of cleaned sample after testing, $\boldsymbol{s}$ is the total surface area ($cm^2$), and $\boldsymbol{t}$ is the testing time (h). The corrosion inhibition efficiency ($\boldsymbol{\eta}$) was determined by Eq. (2):

$$\boldsymbol{\eta} = \frac{\boldsymbol{v_1 - v_2}}{\boldsymbol{v_1}} \quad (2)$$

the $v_1$ is the rate in the 3.5 % NaCl solution, $v_2$ is the rate in the 3.5 % NaCl solution which added corrosion inhibitors.

*2.3. Electrochemical test*

A conventional three electrodes cell was adopted in electrochemical test. A Pt electrode was adopted as the counter electrode (CE), a saturated calomel electrode (SCE) was adopted as reference electrode (RE), and 5052 aluminum alloy was used as working electrode (WE) with 1 $cm^2$ working area. The Corrtest 350 electrochemical workstation was used in electrochemical testing. The frequency used in electrochemical impedance spectroscopy (EIS) test was from 100 kHz to $10^{-2}$ Hz. The amplitude of perturbation potential was 10 mV. The potentials range in polarization curves tests was - 0.3 V ~ 0.3 V (relative to open circuit potentials), and the scanning rate was set to 0.5 mV $s^{-1}$.

*2.4. Surface morphology investigation*

In surface morphology test, 5052 aluminum alloys with size of 2 ×2 ×0.3 cm were grounded by SiC abrasive paper from 400 to 2000 grit, then ultrasonic washed in anhydrous ethanol. After 7-day immersion testing, samples were washed in distilled water and dried. The scanning electron microscope (SEM, Helios NanoLab 600i) with energy dispersive spectrometer (EDS) detector was used to character the surface morphology and elemental composition.

*2.5. Crystal morphology calculation*

Morphology module in Material Studio (MS) software was applied to investigate crystal growth of $CeO_2$ by BFDH algorithm. The energy methods were set to Forcite with 1.0 Å $D_{hkl}$.

*2.6. MC calculation*

The most stable adsorption configuration of L-Arg on $Al_2O_3$ and $CeO_2$ surface was calculated by Adsorption Locator module in MS software. The 4 × 4 $Al_2O_3$ (001) surface (Fig. 1 (a)) and 4 × 4 $CeO_2$ (111) surface (Fig. 1 (b)) was used as adsorption substrate, respectively, and 20 Å vacuum was put to prevent the interference of periodic boundary conditions [31].

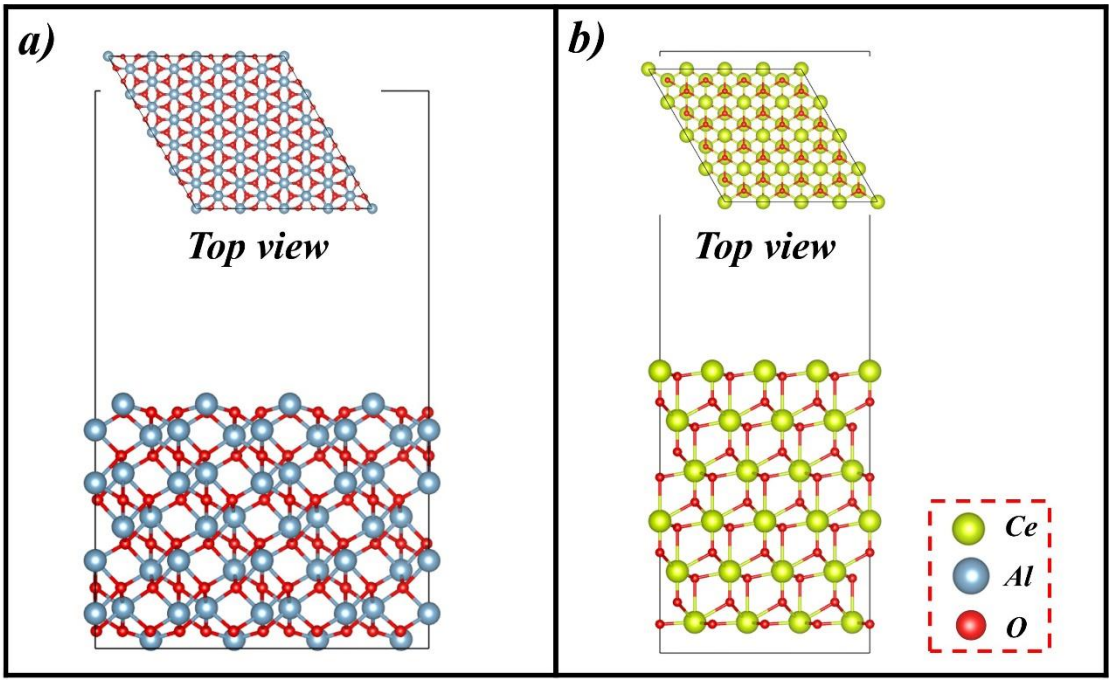


Figure 1. Side view and top view of: (a) $Al_2O_3$ (001) surface; (b) $CeO_2$ (111) surface

COMPASS was used as forcefield in MC calculation, which has been proven suitable to investigated adsorption study [32, 33]. Ewald and atom-based method was used to calculate the electrostatic and van der Waals interaction. The cutting-off distance was adopted to 15.5 Å.

## 3. RESULTS AND DISCUSSION

*3.1. Weight loss test results*

The inhibition efficiency increased when L-Arg was combined with 3 mM $CeCl_3$, indicating that the hybrid inhibitor was more effective than single $CeCl_3$. Combining 3 mM $CeCl_3$ with 4 mM L-Arg could achieve 83.78% inhibition efficiency. However, the efficiency did not increase with L-Arg concentration [34]. S. Therefore, 3 mM $CeCl_3$ and 4 mM L-Arg were the optimal concentrations to reach the maximum efficiency of 83.78%.

Table 1. Weight loss test results of 5052 aluminum alloy in 3.5% NaCl solution without or with different corrosion inhibitors

| Inhibitor | $v$ (mg cm$^{-2}$ h$^{-1}$) | $\eta$ (%) |
|---|---|---|
| blank | $37.1\times10^{-4}$ | - |
| 1 mM $Ce^{3+}$ | $17.3\times10^{-4}$ | 53.37% |
| 2 mM $Ce^{3+}$ | $15.8\times10^{-4}$ | 57.41% |
| 3 mM $Ce^{3+}$ | $14.2\times10^{-4}$ | 61.73% |
| 4 mM $Ce^{3+}$ | $14.6\times10^{-4}$ | 60.65% |
| 3 mM $Ce^{3+}$+2 mM L-Arg | $9.5\times10^{-4}$ | 74.39% |
| 3 mM $Ce^{3+}$+4 mM L-Arg | $6.1\times10^{-4}$ | 83.78% |
| 3 mM $Ce^{3+}$+6 mM L-Arg | $6.3\times10^{-4}$ | 83.02% |

By adding L-Arg with 3 mM $CeCl_3$, the inhibition efficiency increased again, which indicated the hybrid inhibitor was more effective than single $CeCl_3$. Adding 3 mM $CeCl_3$ with 4 mM L-Arg could achieve 83.78 % inhibition efficiency. But the efficiency did not increase with increasing of L-Arg concentration. Therefore, 3 mM $CeCl_3$ with 4 mM L-Arg was the optimal concentration, which can reach the maximum efficiency of 83.78%.

### *3.2. Polarization curve test*

Fig. 2 and Fig. 3 represents the polarization curves testing results, respectively. Relevant polarization curves fitted parameters were presented in Table 2. Study showed the cathode reactions of aluminum alloy in NaCl solution was Eq. (3) and (4) [35, 36].

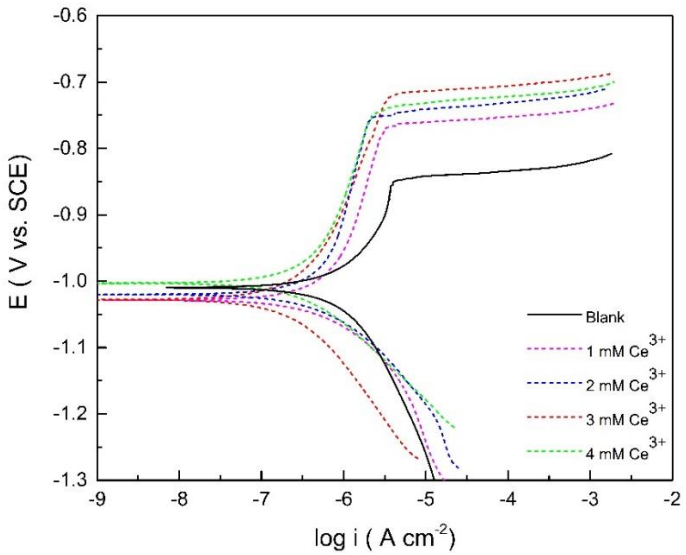


Figure 2. Polarization curves of 5052 aluminum alloy in 3.5 % NaCl solution without or with different concentrations of $CeCl_3$

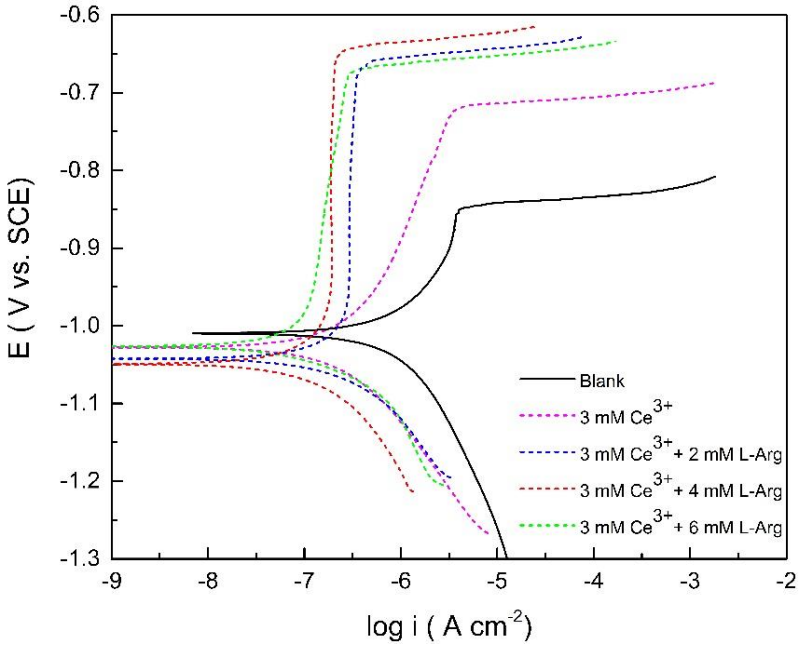


Figure 3. Polarization curves of 5052 aluminum alloy in 3.5 % NaCl solution without or with different concentrations of $CeCl_3$ and L-Arg

Table 2. Polarization curves fitting results of 5052 aluminum alloy in 3.5% NaCl solution without or with different corrosion inhibitors

| Inhibitor | $I_{corr}$ (μA cm$^{-2}$) | $E_{corr}$ (V vs. SCE) | $E_{pit}$ (V vs. SCE) |
|---|---|---|---|
| blank | 2.01 | -1.009 | -0.851 |
| 1 mM $Ce^{3+}$ | 1.09 | -1.025 | -0.768 |
| 2 mM $Ce^{3+}$ | 0.95 | -1.026 | -0.745 |
| 3 mM $Ce^{3+}$ | 0.65 | -1.022 | -0.721 |
| 4 mM $Ce^{3+}$ | 0.71 | -1.004 | -0.742 |
| 3 mM $Ce^{3+}$+2 mM L-Arg | 0.42 | -1.046 | -0.661 |
| 3 mM $Ce^{3+}$+4 mM L-Arg | 0.27 | -1.051 | -0.643 |
| 3 mM $Ce^{3+}$+6 mM L-Arg | 0.29 | -1.019 | -0.668 |

$$O_2 + 2H_2O + 2e^- \rightarrow 2OH_{ads} + 2OH^- \quad (3)$$

$$OH_{ads} + e^- \rightarrow OH^- \quad (4)$$

$OH^-$ formation increased the pH of NaCl solution, and reactions occurred on the aluminum alloy surface as shown in Eqs. (5) and (6) because aluminum is an amphoteric metal element [37].

$$Al_{(s.)ads.} + 3OH^- \rightarrow Al(OH)_{3,ads} + 3e^- \quad (5)$$

$$2Al(OH)_{3,ads} \rightarrow Al_2O_3 \cdot 3H_2O \quad (6)$$

However, $Al_2O_3$ is not stable enough in environments containing $Cl^-$ [38]. $Cl^-$ could attack the weak part of $Al_2O_3$ film, and the aluminum could then dissolve into $Al^{3+}$ as shown in Eq. (7) [39]. $Cl^-$ could interact with $Al^{3+}$ to generate soluble aluminum chloride compounds (Eqs. (8) and (9)) [40], thus increasing the dissolution rate of aluminum. In addition, $Al^{3+}$ could undergo hydrolysis as shown in Eq. (10) [41]; the formation of $H^+$ and the consumption of $OH^-$ in Eqs. (8) and (9) decreased the pH of the anode reaction area. This low pH promoted the diffusion of $Cl^-$ to anode area to maintain electrical neutrality, so the dissolution rate of aluminum alloy was increased. Finally, pitting corrosion occurred on the aluminum alloy.

$$Al - 3e^- \rightarrow Al^{3+} \quad (7)$$

$$Al^{3+} + 4Cl^- \rightarrow AlCl_4^- \quad (8)$$

$$Al^{3+} + 2Cl^- + 2OH^- \rightarrow Al(OH)_2Cl_2^- \quad (9)$$

$$Al^{3+} + 3H_2O \rightarrow Al(OH)_3 + 3H^+ \quad (10)$$

**Error! Reference source not found.** shows that after the addition of different corrosion inhibitors, the change of self-corrosion potential ($E_{corr}$) was less than 150 mV. This finding implied that the hybrid corrosion inhibitor was a mixed-type inhibitor that could decrease the corrosion rate of anode and cathode reactions [37]. Corrosion current density ($I_{corr}$) can be used to judge the corrosion rate. After $CeCl_3$ addition, $I_{corr}$ initially decreased with the increase $CeCl_3$ in concentration, showing that this compound could decrease the corrosion rate of 5052 alloy. Upon the addition of 3 mM $CeCl_3$, $I_{corr}$ decreased form 2.01 μA $cm^{-2}$ (blank solution) to 0.65 μA $cm^{-2}$. Study [42] showed cerium salts occurred reaction as shown in Eq. (11), (12) and (13) to form $CeO_2$ film. The $CeO_2$ film coved the $Al_2O_3$ film and aluminum alloy surface, so the diffusion of $Cl^-$ and reaction sites for corrosion reaction were reduced.

$$4Ce^{3+} + O_2 + 4OH^- + 2H_2O \rightarrow 4Ce(OH)_2^{2+} \quad (11)$$

$$Ce(OH)_2^{2+} + 2OH^- \rightarrow Ce(OH)_4 \quad (12)$$

$$Ce(OH)_4 \rightarrow CeO_2 + 2H_2O \quad (13)$$

Pitting corrosion potential ($E_{pit}$) is also an effective criterion to evaluate the pitting corrosion resistance. An increase in $E_{pit}$ indicated the increasing of pitting corrosion resistance [43]. Adding $CeCl_3$ increased $E_{pit}$ of 5052 aluminum alloy compared with that in blank solution, and $E_{pit}$ increased form – 0.851 V (blank solution) to – 0.721 V when adding 3 mM $CeCl_3$. This showed adding $CeCl_3$ can significantly increase pitting corrosion resistance for 5052 aluminum alloy. But when adding $CeCl_3$ over 3 mM, the $I_{corr}$ and $E_{pit}$ did not significant change with the increasing of concentration of $CeCl_3$, so the optimal concentration for $CeCl_3$ was 3 mM, which was consistence with weight loss test results.

$I_{corr}$ decreased again when $CeCl_3$ was combined with L-Arg, indicating that the hybrid corrosion inhibitor had better inhibition ability than single $CeCl_3$. When 3 mM $CeCl_3$ was combined with 4 mM L-Arg, $I_{corr}$ decreased from 2.01 μA $cm^{-2}$ (blank solution) to 0.27 μA $cm^{-2}$ and $E_{pit}$ increased from − 0.851 V (blank solution) to − 0.643 V. This finding showed that the hybrid inhibitor effectively decreased

the corrosion rate and increased the pitting corrosion resistance of 5052 aluminum alloy. The $I_{corr}$ and $E_{pit}$ did not significant change when adding more than 4 mM L-Arg. Therefore, the optimal concentrations for the hybrid inhibitor were 3 mM $CeCl_3$ and 4 mM L-Arg, which were the same as the result of weight loss test.

### *3.3. EIS test results*

EIS results are shown in Fig. 4 and Fig. 5, respectively. Fig. 6 showed the equivalent circuit model adopted in the EIS fitting. The $R_s$ is the solution resistance.

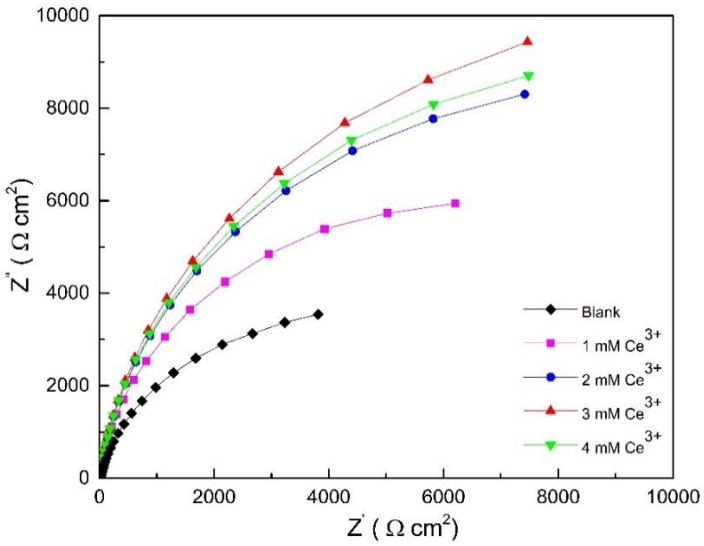


Figure 4. EIS results of 5052 aluminum alloy in 3.5 % NaCl solution without or with different concentrations of $CeCl_3$

Constant phase angle element (CPE) was adopted to study the performance of the electric double layer capacitor given the real surface not being ideal surface [44]. $R_{ct}$ represents the change transfer resistance on aluminum alloy surface, and is a useful parameter to evaluate the corrosion inhibition efficiency. A large $R_{ct}$ corresponds to a high charge transfer resistance, making corrosion difficult to proceed [45]. EIS fitting results for 5052 aluminum alloy in 3.5% NaCl solution without or with different corrosion inhibitors are shown in Table 3.

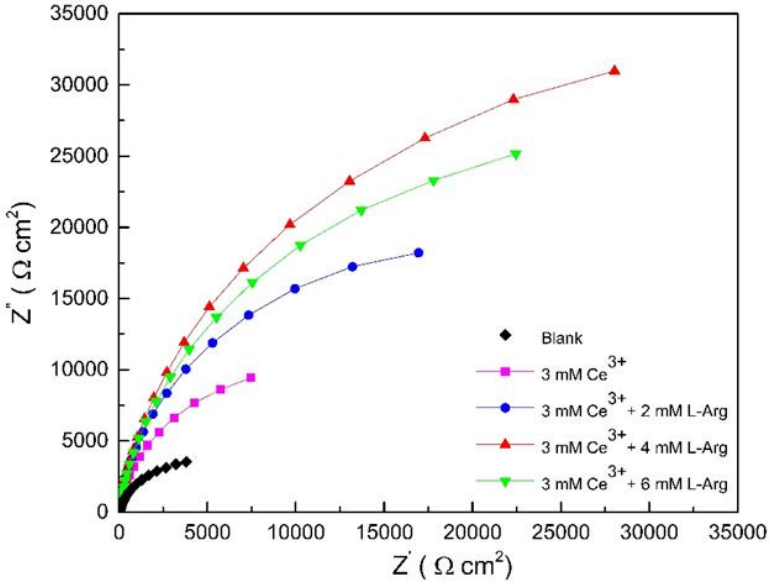


Figure 5. EIS results of 5052 aluminum alloy in 3.5 % NaCl solution without or with different concentrations of $CeCl_3$ and L-Arg

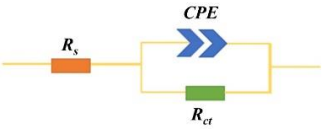


**Figure 1**. Equivalent circuit model used in EIS study

Table 3. EIS fitting results of 5052 aluminum alloy in 3.5% NaCl solution without or with different corrosion inhibitors

| Inhibitor | $R_S$ ($\Omega$ cm$^2$) | CPE | | $R_{ct}$ ($\Omega$ cm$^2$) |
|---|---|---|---|---|
| | | $Y_0$(Ss$^n$ cm$^{-2}$) | n | |
| blank | 4.55 | $4.51 \times 10^{-5}$ | 0.87 | 8523 |
| 1 mM $Ce^{3+}$ | 5.31 | $1.72 \times 10^{-5}$ | 0.92 | 13376 |
| 2 mM $Ce^{3+}$ | 5.42 | $1.51 \times 10^{-5}$ | 0.91 | 20019 |
| 3 mM $Ce^{3+}$ | 5.62 | $1.48 \times 10^{-5}$ | 0.92 | 23970 |
| 4 mM $Ce^{3+}$ | 5.71 | $1.52 \times 10^{-5}$ | 0.92 | 21845 |
| 3 mM $Ce^{3+}$+2 mM L-Arg | 5.12 | $4.66 \times 10^{-6}$ | 0.95 | 38673 |

| | | | | |
|---|---|---|---|---|
| 3 mM $Ce^{3+}$+4 mM L-Arg | 6.09 | $5.56 \times 10^{-6}$ | 0.94 | 66391 |
| 3 mM $Ce^{3+}$+6 mM L-Arg | 6.78 | $5.68\times 10^{-6}$ | 0.94 | 56046 |

According to Figs. 4 and 5, and **Error! Reference source not found.**, $R_{ct}$ increased with $CeCl_3$ addition compared with that in the blank solution. Upon the addition of 3 mM $CeCl_3$, $R_{ct}$ increased from 8523 Ω $cm^2$ (blank solution) to 23970 Ω $cm^2$, showing that $CeCl_3$ increased the charger transfer resistance of 5052 aluminum alloy to hinder corrosion. However, $R_{ct}$ did not increase again when the $CeCl_3$ concentration was over 3 mM. Hence, the optimal concentration for $CeCl_3$ was 3 mM, which was the same as the results of weight loss test and polarization curves test. $R_{ct}$ increased again when L-Arg was combined with 3 mM $CeCl_3$, indicating that the hybrid inhibitor was more effective than single $CeCl_3$.When 3 mM $CeCl_3$ was combined with 4 mM L-Arg, $R_{ct}$ increased from 8523 Ω $cm^2$ (blank solution) to 66391 Ω $cm^2$. Therefore, the hybrid inhibitor effectively increased the charger transfer resistance, so corrosion was hindered. However, $R_{ct}$ did not increase again when more than 4 mM L-Arg was added, so the optimal concentrations for the hybrid inhibitor were 3 mM $CeCl_3$ and 4 mM L-Arg.

### *3.4. SEM and EDS test results*

The corrosion inhibition effect of corrosion inhibitor can be intuitively evaluated by observing the corrosion morphology [46]. Additionally, by detecting the elements composition can analyze the composition of corrosion products and corrosion inhibitor film [47]. Surface morphology of 5052 alloy after the immersion testing are shown in Fig. 7. Element composition (wt %) for sites marked in Fig. 7 were shown in Table 4.

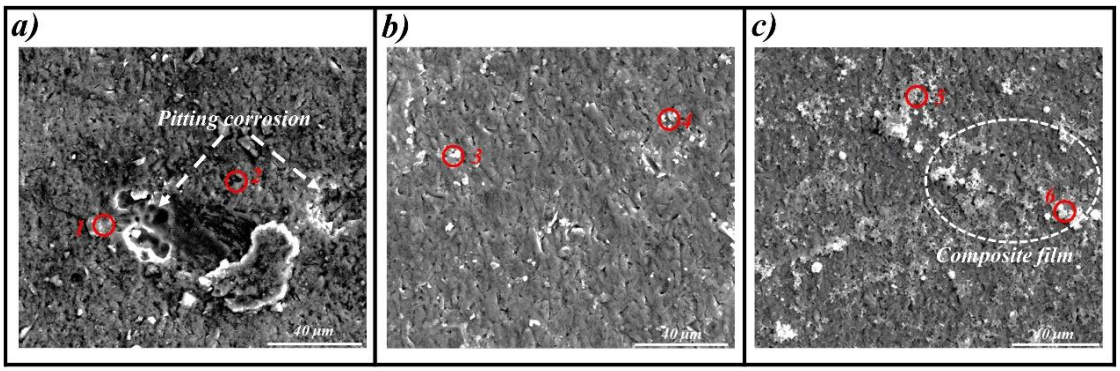


Figure 7. Surface morphology of 5052 aluminum alloy after a 7-day immersion test in 3.5 % NaCl solution without or with different corrosion inhibitors: (a) 3.5 % NaCl solution; (b) 3.5 % NaCl solution added 3 mM $CeCl_3$; (c) 3.5 % NaCl solution added 3 mM $CeCl_3$ with 4 mM L-Arg

Table 4. Element composition (wt %) of the sites marked in **Error! Reference source not found.**

| Area | Composition (wt %) | | | | | |
|---|---|---|---|---|---|---|
| | Al | O | Ce | N | C | Cl |
| 1 | 86.62 | 11.23 | - | - | - | 2.15 |
| 2 | 93.63 | 6.02 | | - | - | 0.35 |
| 3 | 50.41 | 31.23 | 18.23 | - | - | 0.13 |
| 4 | 56.88 | 33.24 | 9.76 | - | - | 0.12 |
| 5 | 34.19 | 26.32 | 30.61 | 3.21 | 5.67 | - |
| 6 | 30.05 | 28.63 | 32.15 | 2.96 | 6.21 | - |

After a 7-day immersion testing, the sample in blank solution showed obvious pitting corrosion (Fig.7 (a)), implying that the $Al_2O_3$ film formed on 5052 aluminum alloy could not prevent the corrosion of $Cl^-$. As shwon in Table 4, the $Cl^-$ content on site 1 (near pitting corrosion site) was much higher than that on site 2 (non-pitting corrosion site), indicating that the enrichment and diffusion of $Cl^-$ was the main reason for pitting corrosion [48]. For the sample in 3.5 % NaCl soultion with 3 mM $CeCl_3$, no obvious pitting corrosion was observed (Fig.7 (b)), showing that the $CeO_2$ film effectively hindered the diffusion of $Cl^-$ and blocked the corrosion site for 5052 aluminum alloy. In sites 3 and 4, Ce element was detected, proving that the $CeO_2$ film was formed bbut was not dense enough. After 3 mM $CeCl_3$ was combined with 4 mM L-Arg, a dense film was formed on 5052 aluminum alloy surfaces (Fig.7 (c)) and no pitting corrosion sites were observed. Ce, N, and C elements were detected in sites 5 and 6, suggesting the formation of $CeO_2$/Al2$O_3$–L-Arg complex film that effectively prevented the diffusion of $Cl^-$ and blocked the corrosion sites on 5052 aluminum alloy. Hence, the hybrid inhibitor showed good corrosion inhibition efficiency.

*3.5. Crystal morphology calculation results*

Before adsorption calculation, suitable adsorption surface for corrosion inhibitor molecules should be chosen. According to a previous study, the most stable surface was suitable as adsorption study [49]. Previous study [50] showed the most stable surface of $Al_2O_3$ was (001) surface, so (001) surface was chosen as adsorption substrate for $Al_2O_3$. For $CeO_2$, the growth morphology of $CeO_2$ calculated by the BFDH method was shown in Fig. 8.

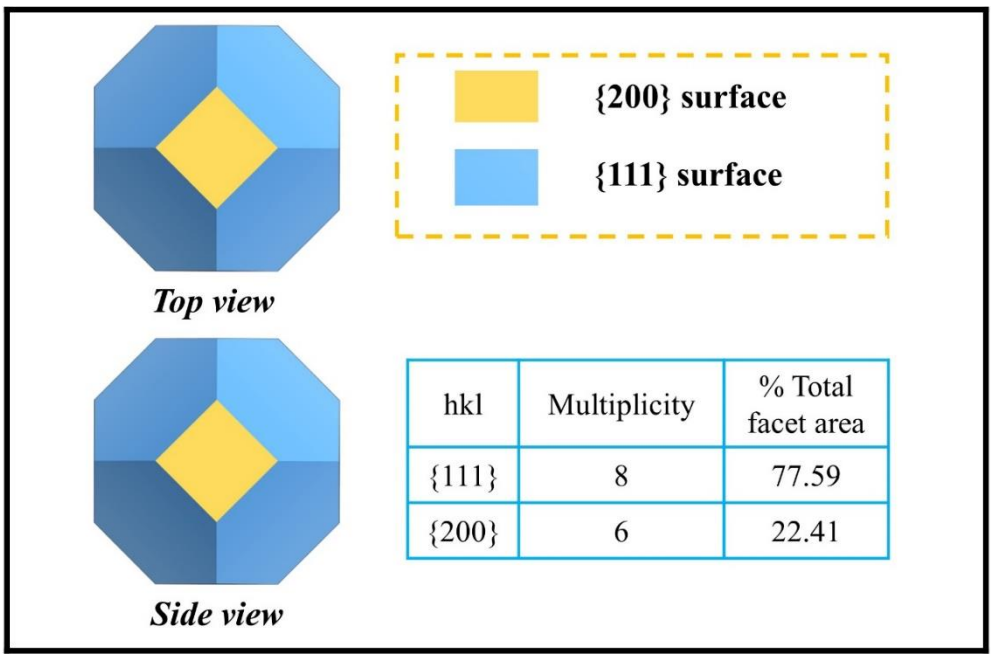


Figure 8. The growth morphology of $CeO_2$ calculated by the BFDH method

The {111} surface occupied 77.59 % total surface area while {002} was only 22.41%, which indicated that {111} surface was the most stable surface for $CeO_2$. Additionally, the multiplicity of {111} and {002} surface was 8 and 6, respectively. Previous study [49] showed surface with large multiplicity number was more suitable as adsorption substrate due to large multiplicity number can provide more adsorption sites for corrosion inhibitor molecules. Therefore, {111} surface was chosen as adsorption sites for $CeO_2$.

### *3.6. Monte Carlo calculation results*

As shown in the previous results, the well corrosion inhibition performance was mainly due to the formation of $CeO_2$/$Al_2O_3$–L-Arg complex film. To systematically reveal the inhibition mechanism, adsorption behavior of L-Arg on $CeO_2$ and $Al_2O_3$ surface was investigated by MC calculation at atomic level.

The most stable configurations and relative adsorption energy are shown in Fig. 9 (a) and (b), respectively.

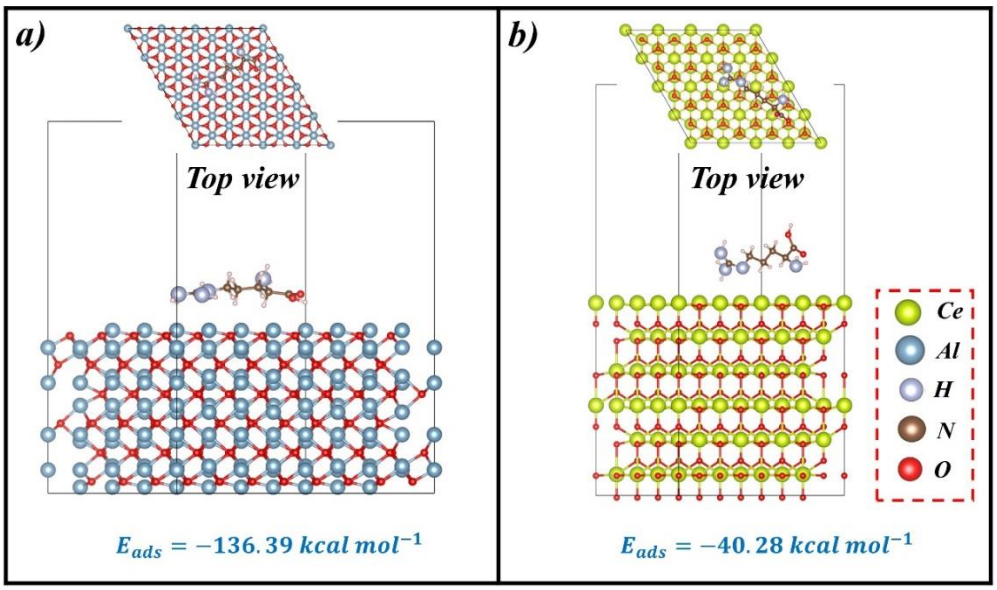


Figure 9. The most stable configurations and adsorption energy calculated by MC simulation for L-Arg on: (a) $Al_2O_3$ (001) surface; (b) $CeO_2$ (111) surface

The L-Arg molecule presented a parallel adsorption configuration on two surfaces. Previous study [51] showed the parallel adsorption configuration could cover more surface area, which was helpful for preventing the diffusion of corrosive particles. Our previous electrostatic potential calculation results [25] for L-Arg molecule showed the active sites on L-Arg was N and O atoms, so it can be seen the adsorption was mainly caused by the N and O atoms on L-Arg. Adsorption energy was useful to evaluate the adsorption strength of corrosion inhibitor molecules. A negative value meant the adsorption was spontaneous [52]. The L-Arg adsorption energy on each surface was negative, indicating L-Arg molecules could spontaneously adsorbed on $CeO_2$ and $Al_2O_3$ surface to form $CeO_2$/$Al_2O_3$–L-Arg complex film. Additionally, the absolute value of adsorption energy can be used quantitatively to evaluate adsorption strength. A larger absolute value corresponding to a greater adsorption strength [53]. The absolute value of adsorption energy for L-Arg on $CeO_2$ (111) surface was significantly larger than that of $Al_2O_3$ (001) surface. Therefore, the formation of $CeO_2$ promote the adsorption of L-Arg, and $CeO_2$–L-Arg complex film was more stable than $Al_2O_3$–L-Arg film. Finally, the hybrid inhibitor formed stable complex film that effectively prevent the diffusion of $Cl^-$ and blocked the active corrosion area.

### *3.7. Corrosion inhibition mechanism*

The corrosion mechanism diagrams of 5052 aluminum alloy in different solutions are shown in Fig. 10. As displayed in Fig. 10 (a), an $Al_2O_3$ film was formed on 5052 aluminum alloy in 3.5 % NaCl solution. The cathode area was alkaline due to the $OH^-$ generated from cathode reaction. However, the $Al_2O_3$ film was not stable in the presence of $Cl^-$. The broken area of $Al_2O_3$ film led to the dissolution of Al to $Al^{3+}$, and $Cl^-$ reacted with $Al^{3+}$ to form a soluble aluminum chloride compound, which promoted the dissolution of aluminum. In addition, the $Al^{3+}$ underwent hydrolysis to form $Al(OH)_3$ and $H^+$. The

formation of $H^+$ and the consumption of $OH^-$ promoted the diffusion of $Cl^-$ to maintain electrical neutrality enhanced the dissolution of aluminum, and caused the anode area to become acidic. The small acid anode area and large alkaline cathode area formed the corrosion battery, finally causing the severe pitting corrosion of 5052 aluminum alloy [54].

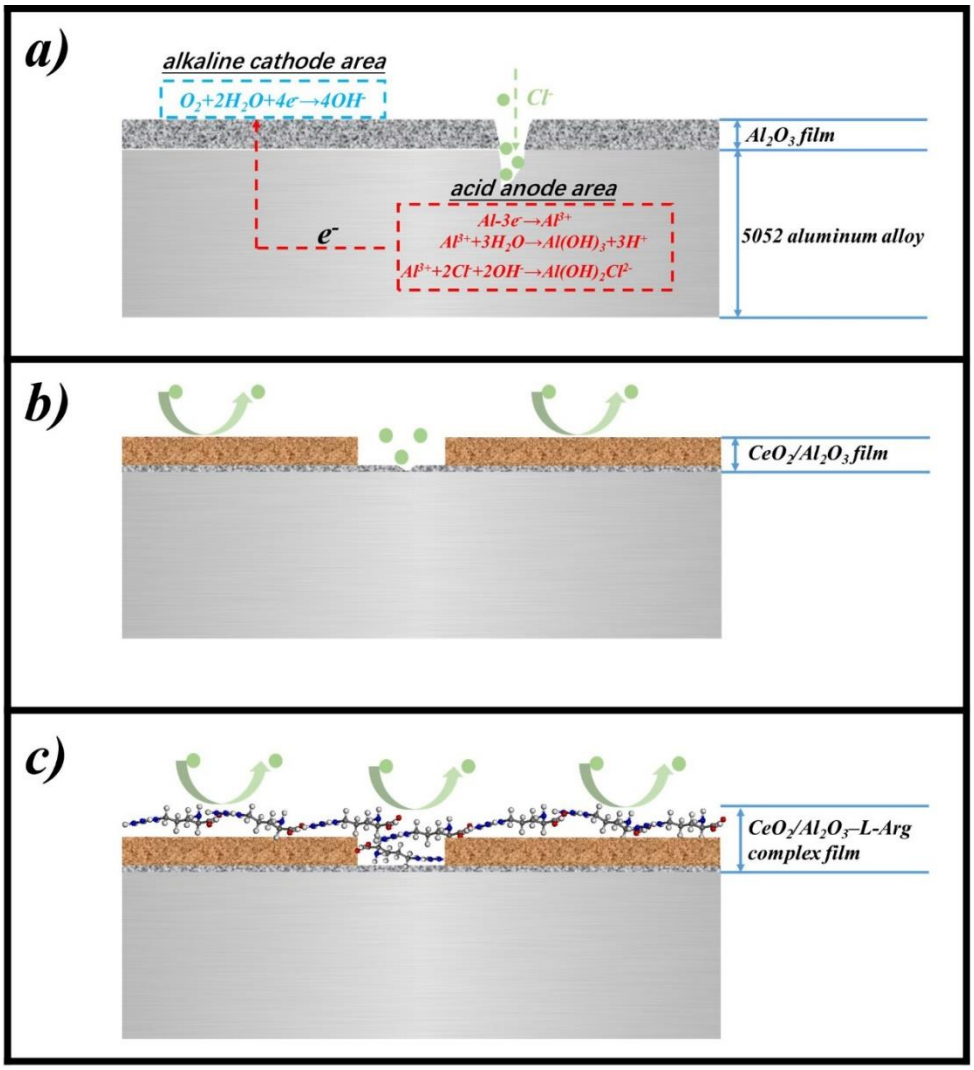


Figure 10. Corrosion mechanism diagrams of 5052 aluminum alloy in different solutions: (a) 3.5 % NaCl solution; (b) 3.5 % NaCl solution adding 3 mM $CeCl_3$; (c) 3.5 % NaCl solution adding 3 mM $CeCl_3$ with 4 mM L-Arg

After $CeCl_3$ was added to 3.5 % NaCl solution (Fig. 10 (b)), the $CeO_2$ film formed on 5052 aluminum alloy blocked the corrosion reaction sites and prevented the diffusion of $Cl^-$ to decreased the corrosion rate. However, the single $CeO_2$ film was not dense enough, and some areas that were not covered by $CeO_2$ were still relatively weak. After the $CeCl_3$/L-Arg hybrid corrosion inhibitor was added to 3.5 % NaCl solution (Fig. 10 (c)), L-Arg was adsorbed on $CeO_2$ and $Al_2O_3$ film to form $CeO_2/Al_2O_3$–L-Arg complex film. This complex film was dense so it effectively prevented the diffusion of $Cl^-$ and blocked the active corrosion reaction sites. Therefore, the $CeCl_3$/L-Arg hybrid corrosion inhibitor showed good corrosion inhibition efficiency for 5052 aluminum alloy in 3.5 % NaCl solution.

## 4. CONCLUSIONS

The corrosion inhibition behavior of a novel $CeCl_3$/L-Arg hybrid corrosion inhibitor for 5052 aluminum alloy in 3.5% NaCl solution was systematically studied by the combination of experimental and theoretical methods. The conclusions were as follows:

1) Both single $CeCl_3$ and $CeCl_3$/L-Arg hybrid corrosion inhibitor could decrease the corrosion rate of 5052 aluminum alloy in 3.5 % NaCl solution. Adding 3 mM $CeCl_3$ and 4 mM L-Arg could reach the highest corrosion inhibition efficiency of 83.78%.

2) Polarization curve results showed the hybrid inhibitor was a mixed-type inhibitor. In the optimal concentration, the $E_{pit}$ increased by 208 mV compared with that of blank solution, which significantly improved the pitting corrosion resistance for 5052 aluminum alloy. EIS results showed the hybrid corrosion inhibitor effectively increased the charge transfer resistance, which hindered corrosion process.

3) Crystal morphology calculation showed the most stable surface of $CeO_2$ was {111} surface and MC simulation results showed $CeO_2$ film increased adsorption energy of L-Arg molecules compared with $Al_2O_3$ film.

4) Combining the experimental and theoretical results, the inhibition ability of hybrid inhibitor was attributed to the formation of $CeO_2$/$Al_2O_3$–L-Arg complex films, which dramatically hindered the diffusion of $Cl^-$ and blocked active corrosion sites.

ACKNOWLEDGEMENTS

This work was supported by the National Natural Science Foundation of China (under grant No. 51974091), National Science Foundation of Heilong Jiang Province (under grant No. LH2019E021).

## References

1. F.S. Hung, *Emerg. Mater. Res*., 9 (2020) 750-757.
2. X. Chen, Y.M. Xia, F. Zhuang, Z. Liu, Z.M. Gao, *Int. J. Electrochem. Sci*., 16 (2021).
3. J. Yang, D. Zhang, T. Lin, W. Zhang, C. Li, L. Gao, *J. Taiwan Inst. Chem. Eng*., 131 (2022) 104150.
4. F. Feng, J. Li, P. Yuan, Q. Zhang, P. Huang, H. Su, R. Chen, *Metals*, 8 (2018) 761.
5. M.F. Naeini, M.H. Shariat, M. Eizadjou, *J. Alloys Compd*., 509 (2011) 4696-4700.
6. E.B. Moustafa, A.O. Mosleh, *J. Alloys Compd*., 823 (2020) 153745.
7. H.A. Almashhadani, M.K. Alshujery, M. Khalil, M.M. Kadhem, A.A. Khadom, *J. Mol. Liq*., 343 (2021) 117656.
8. I. Mohammadi, T. Shahrabi, M. Mahdavian, M. Izadi, *J. Mol. Liq.*, 307 (2020) 112965.
9. B.G. Prakashaiah, D. Vinaya Kumara, A. Anup Pandith, A. Nityananda Shetty, B.E. Amitha Rani, *Corros. Sci*., 136 (2018) 326-338.
10. D.K. Kozlica, A. Kokalj, I. Milošev, *Corros. Sci*., 182 (2021) 109082.
11. M. Radi, R. Melian, M. Galai, N. Dkhirche, M. Makha, C. Verma, C. Fernandez, M. EbnTouhami, *J. Mol. Liq.*, 337 (2021) 116547.
12. G.O. Ilevbare, G.T. Burstein, *Corros. Sci*., 45 (2003) 1545-1569.
13. M. Becker, *Corros. Rev*., 37 (2019) 321-342.

14. X.T. Xu, H.W. Xu, Y.F. Cui, W. Li, Y. Wang, X.Y. Zhang, *J. Mol. Model.*, 28 (2022) 55.
15. A. Marciales, T. Haile, B. Ahvazi, T.D. Ngo, J. Wolodko, *Corros. Rev*., 36 (2018) 239-266.
16. C. Verma, E.E. Ebenso, I. Bahadur, M.A. Quraishi, *J. Mol. Liq.*, 266 (2018) 577-590.
17. A.E. Somers, B.R.W. Hinton, C. de Bruin-Dickason, G.B. Deacon, P.C. Junk, M. Forsyth, *Corros. Sci*., 139 (2018) 430-437.
18. D. Mohammedi, F. Ismail, R. Rehamnia, R. Bensalem, O. Savadogo, *Corros. Eng. Sci. Technol*., 50 (2015) 633-638.
19. T. Hu, H. Shi, D. Hou, T. Wei, S. Fan, F. Liu, E.-H. Han, *Appl. Surf. Sci*., 467-468 (2019) 1011-1032.
20. T. Matsuda, K.B. Kashi, K. Fushimi, V.J. Gelling, *Corros. Sci*., 148 (2019) 188-197.
21. M.A. Deyab, S.S.A. El-Rehim, H.H. Hassan, A.M. Shaltot, *J. Alloys Compd*., 820 (2020) 153428.
22. F. Ivušić, O. Lahodny-Šarc, H.O. Ćurković, V. Alar, *Corros. Sci.*, 98 (2015) 88-97.
23. Y. Zhang, S. Zhang, B. Tan, L. Guo, H. Li, *J. Colloid Interface Sci*., 604 (2021) 1-14.
24. Q.X. Kang, Y. Wang, X.Y. Zhang, *J. Alloys Compd*., 774 (2019) 1069-1080.
25. X.T. Xu, H.W. Xu, W. Li, Y. Wang, X.Y. Zhang, *J. Mol. Liq.*, 345 (2022) 117010.
26. B. El Ibrahimi, A. Jmiai, L. Bazzi, S. El Issami, *Arabian J. Chem*., 13 (2020) 740-771.
27. I.B. Obot, K. Haruna, T.A. Saleh, *Arab. J. Sci. Eng*., 44 (2019) 1-32.
28. C. Verma, H. Lgaz, D.K. Verma, E.E. Ebenso, I. Bahadur, M.A. Quraishi, *J. Mol. Liq*., 260 (2018) 99-120.
29. E.E. Ebenso, C. Verma, L.O. Olasunkanmi, E.D. Akpan, D.K. Verma, H. Lgaz, L. Guo, S. Kaya, M.A. Quraishi, *Phys. Chem. Chem. Phys*., 23 (2021) 19987-20027.
30. O. Dagdag, Z. Safi, H. Erramli, N. Wazzan, I.B. Obot, E.D. Akpan, C. Verma, E.E. Ebenso, O. Hamed, A. El Harfi, *J. Mol. Liq*., 287 (2019) 110977.
31. Q. Kang, G. Wang, Q. Liu, X. Sui, Y. Liu, Y. Chen, S. Luo, Z. Li, *Corros. Sci*., 191 (2021) 109756.
32. M.S. Masoud, M.K. Awad, A.E. Ali, M.M.T. El-Tahawy, *J. Mol. Struct*., 1063 (2014) 51-59.
33. S.N. Costa, F.W.Q. Almeida-Neto, O.S. Campos, T.S. Fonseca, M.C. de Mattos, V.N. Freire, P. Homem-de-Mello, E.S. Marinho, N.K.V. Monteiro, A.N. Correia, P. de Lima-Neto, *J. Mol. Liq*., 326 (2021) 115330.
34. J. Liu, D. Wang, L. Gao, D. Zhang, *Appl. Surf. Sci*., 389 (2016) 369-377.
35. D.Q. Zhang, X. Jin, B. Xie, H. Goun Joo, L.X. Gao, K.Y. Lee, *Surf. Interface Anal*., 44 (2012) 78-83.
36. E.S.M. Sherif, *Int. J. Electrochem. Sci*., 6 (2011) 1479-1492.
37. K. Zhang, W. Yang, B. Xu, Y. Chen, X. Yin, Y. Liu, H. Zuo, *J. Colloid Interface Sci*., 517 (2018) 52-60.
38. A. Singh, Y. Lin, W. Liu, S. Yu, J. Pan, C. Ren, D. Kuanhai, *J. Ind. Eng. Chem*., 20 (2014) 4276-4285.
39. E.M. Sherif, S.-M. Park, *Electrochim. Acta*, 51 (2006) 1313-1321.
40. Z. Szklarska-Smialowska, *Corros. Sci*., 41 (1999) 1743-1767.
41. M. Machkova, E.A. Matter, S. Kozhukharov, V. Kozhukharov, *Corros. Sci*., 69 (2013) 396-405.
42. C. Zhu, H.X. Yang, Y.Z. Wang, D.Q. Zhang, Y. Chen, L.X. Gao, *Ionics*, 25 (2019) 1395-1406.
43. H.-Y. Ha, T.-H. Lee, C.-G. Lee, H. Yoon, *Corros. Sci*., 149 (2019) 226-235.
44. X. Zheng, T. Zhang, H. Yang, Q. Zheng, Y. Gao, Z. Liu, W. Wang, K. Wang, *Electrochim. Acta*, 354 (2020) 136635.
45. R. Padash, G.S. Sajadi, A.H. Jafari, E. Jamalizadeh, A.S. Rad, *Mater. Chem. Phys*., 244 (2020) 122681.
46. J. Zhou, X. Niu, Y. Cui, Z. Wang, J. Wang, R. Wang, *Appl. Surf. Sci*., 505 (2020) 144507.
47. C. Zhu, H. Yang, A. Wu, D. Zhang, L. Gao, T. Lin, *J. Power Sources*, 432 (2019) 55-64.
48. M. Ostapiuk, J. Bieniaś, *Adv. Eng. Mater*., 23 (2021) 2001030.
49. X.Y. Zhang, Q.X. Kang, Y. Wang, *Comput. Theor. Chem*., 1131 (2018) 25-32.
50. W. Gong, X.C. Li, B.Q. Zhu, *Materials*, 10 (2017).

51. Q.X. Kang, T.Y. Zhang, X. Wang, Y. Wang, X.Y. Zhang, *J. Power Sources*, 443 (2019) 227251.
52. Q. Kang, G. Wang, Q. Liu, X. Sui, Y. Liu, Y. Chen, S. Luo, Z. Li, *Vacuum*, 193 (2021) 110522.
53. Q. Kang, G. Wang, Q. Liu, X. Sui, Y. Liu, Y. Chen, S. Luo, Z. Li, *J. Alloys Compd*., 885 (2021) 160940.
54. D. Wang, D. Yang, D. Zhang, K. Li, L. Gao, T. Lin, *Appl. Surf. Sci*., 357 (2015) 2176-2183